Author for correspondence:
Neil Curtis
e-mail: n.curtis@hull.ac.uk

# Cranial sutures work collectively to distribute strain throughout the reptile skull

Neil Curtis[1], M. E. H. Jones[2], S. E. Evans[2], P. O'Higgins[3] and M. J. Fagan[1]

[1]Medical and Biological Engineering Research Group, School of Engineering, University of Hull, Hull HU6 7RX, UK
[2]Research Department of Cell and Developmental Biology, University College London, Gower Street, London WCIE 6BT, UK
[3]Centre for Anatomical and Human Sciences, Hull York Medical School, University of York, York YO10 5DD, UK

The skull is composed of many bones that come together at sutures. These sutures are important sites of growth, and as growth ceases some become fused while others remain patent. Their mechanical behaviour and how they interact with changing form and loadings to ensure balanced craniofacial development is still poorly understood. Early suture fusion often leads to disfiguring syndromes, thus is it imperative that we understand the function of sutures more clearly. By applying advanced engineering modelling techniques, we reveal for the first time that patent sutures generate a more widely distributed, high level of strain throughout the reptile skull. Without patent sutures, large regions of the skull are only subjected to infrequent low-level strains that could weaken the bone and result in abnormal development. Sutures are therefore not only sites of bone growth, but could also be essential for the modulation of strains necessary for normal growth and development in reptiles.

## 1. Introduction

Skulls are made up of many bones that are connected by fibrocellular joints at sutures [1–6]. While the term 'suture' is sometimes used to refer solely to the soft tissue component of the joint [7], we use this term to include both the soft tissue component and the bone at the suture edges [8]. Sutures are sites of appositional bone growth [4,6,9–12] and are crucial in the developing skull, where their premature fusion can lead to abnormal growth [13–18]. As skulls mature, the sutures may become fused yet some remain patent throughout life [1,19], suggesting that they have an additional role. In some non-mammalian tetrapods, the joint between bones at patent sutures can be so large and flexible that the suture contributes to movements within the skull [20,21]. Nonetheless, more generally, the retention of patent sutures in mature skulls is thought to be related to stress transfer and/or stress dampening [5,22,23]. However, although the relative importance of each of these roles continues to be debated, their possible interactions merit more serious consideration. Thus, during growth patent sutures contribute not only to bone apposition but, given their patency and physical properties, must inevitably also impact on skull mechanics as they do in adults. In turn, the contribution of sutures to load transfer and to stress and strain modification within the skull [24–27] is likely to impact on cranial bone growth [28].

Virtual computational techniques such as finite-element analysis (FEA) are ideally suited to investigating the impact of patent sutures on skull stresses and strains. The established way to measure strains experimentally is with strain gauges fixed to the surface of bones [29–35]. Local strain at these specific locations is returned, but inferring either strain over the whole skull or the function of patent sutures is problematic. FEA allows stresses and strains to be predicted for the entire structure [36–44], and anatomical features to be controlled so that the influence of patent or fused sutures can be explored [45–51]. Moazen *et al.* [24] carried out such an analysis on a lizard skull, where specific sutures were modelled as patent within the computer model
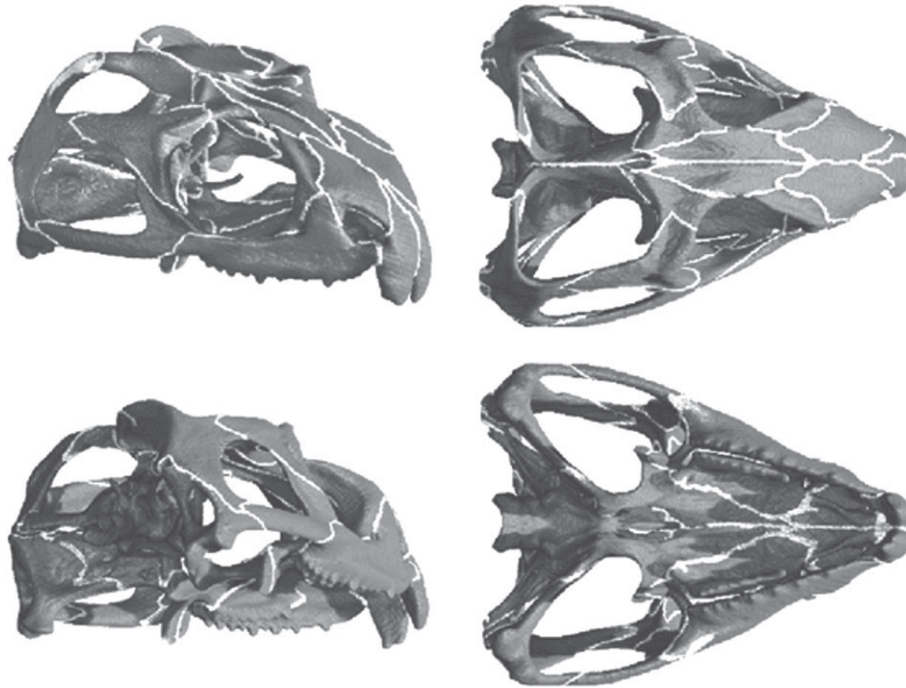
**Figure 1.** The skull model of the reptile *Sphenodon*. Grey regions of the skull represent bone material and white regions represent suture material.

and their impact on local and global strains assessed. This study revealed that patent sutures modified strains over the skull compared with fused sutures, and that whereas strains decreased in some areas of the skull, they increased in others. However, Wang *et al.* [52] concluded that patent sutures have little effect on skull strains in primates, and that they are perhaps less important mechanically than in animals with more patent sutures or a greater suture to bone volume, such as lizards and alligators [24,53]. Such studies combined with experimental data provide important information on suture form and function [3,23,29,30,32,54], but for a full overview of the impact of patent and fused sutures on load transfer within the skull more comprehensive analyses are necessary. The skull experiences loads of varying location, direction and magnitude during normal everyday activities such as feeding, and the same is true for sutures. To appreciate fully the function or impact of sutures on skull stresses and strains, a range of loading regimens should be investigated. However, this was not done in previous studies.

Past work has suggested that: patent sutures do not affect strain distributions [52]; patent sutures act as strain sinks and reduce strains [22,23]; sutures both reduce and elevate strains [24] and that patent sutures help modulate strains throughout the skull [30,55,56]. Here, we investigate the impact of experimental, *in silico*, fusion of sutures on strain magnitudes and distributions within the skull of the reptile *Sphenodon* by testing the following hypotheses.

Hypothesis 1: sutures have no impact on strain distribution and magnitude in the skull.
Hypothesis 2: patent sutures reduce the mean strain across the skull.
Hypothesis 3: patent sutures lead to more uniform strain distributions in the skull.

To do this, we combine two computational techniques, multibody dynamics analysis (MDA) and FEA in the reptile *Sphenodon*, first to predict 15 separate biting loading regimens, and then to analyse the structural performance of the skull under these. The performance of the skull under many

different loading regimens is important because the skull will deform differently dependent upon the loading position and magnitude. This is a consideration most other studies do not take into account.

There are over 100 sutural joints in the skull of *Sphenodon* [3], and all patent sutures were carefully incorporated into the model (figure 1). This level of suture modelling has not been carried out before. The deformation of each individual suture will impact on all other sutures, thus excluding one or more sutures from the model may affect the deformations of both the bones and the other sutures. Understanding the role of sutures with respect to load transfer in the skull of *Sphenodon*, where sutural anatomy is complex, can provide important information on general skull mechanics. In addition, identifying the overall contribution of patent sutures to load transfer through the skull may improve our understanding of medical conditions such as craniosynostosis, where skull growth is abnormal due to early suture fusion.

## 2. Material and methods

### 2.1. Multibody dynamics analysis

Detailed descriptions of the MDA model development have been presented elsewhere [57–61]. Briefly, the cranium and lower jaws (left and right parts) of a *Sphenodon* skull (specimen ID: LDUCZ x036) were scanned in-house by micro-computed tomography (micro-CT), and three-dimensional geometries were constructed using AMIRA image segmentation software (AMIRA v. 4.1, Mercury Computer Systems Inc. USA). Neck vertebral geometries were generated from additional micro-CT scans (specimen YPM 9194—University of Texas, Austin, USA). These three-dimensional geometries were imported into ADAMS multibody analysis software (MSC Software Corp. USA) in preparation for an MDA. The skull had representative dimensions of length 68 mm, width 56 mm and height 35 mm. The total volume of the skull (including the bone and the sutures—as represented in figure 1) was approximately 10 160 mm$^3$. Within ADAMS, detailed muscle anatomy was incorporated onto the geometries,
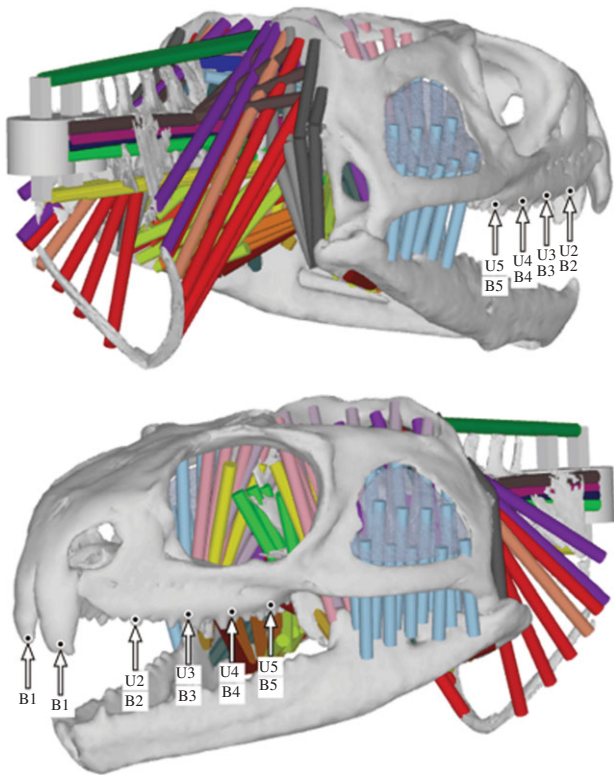
**Figure 2.** The MDA model highlighting bite location and type. U, unilateral bite; B, bilateral bite. Two ripping bites were also simulated at B2.

and accurate jaw joint and tooth contact surfaces were specified. Where the neck met the skull a spherical joint was assigned that permitted the skull to rotate freely about all axes while constraining translational movements. The major adductor (jaw closing), depressor (jaw opening) and neck musculature were included, with each muscle group split into several sections and defined over the anatomical origin and insertions areas on the skull and lower jaws, respectively [57,60,62] (figure 2). To permit biting, a food bolus was modelled that could be located at any position along the jaw, and a specially developed motion technique, named dynamic geometric optimization [62], was used to simulate typical feeding movements. Simply, the line of action of each muscle is used to determine its level of activity during jaw movements. This motion technique, along with the muscle forces and biting performance, has been described and validated elsewhere [58,59,62].

Fifteen biting simulations were performed, including eight unilateral bites, five bilateral bites and two ripping bites (figure 2, as in [36]). During all bites, the adductor muscles were fully activated to ensure peak bite forces were generated. The ripping bites aimed to pull the head dorsally to the left, and dorsally to the right while biting down onto a fixed food bolus. This caused neck muscle forces to reach their maximum magnitudes. In all simulations, the lower jaws opened from a closed position to allow the food bolus to locate unobstructed at a specified tooth location. The lower jaws then closed to contact the food, upon which forces within all adductor muscle groups were ramped up until they reached their peak magnitudes. The MDA outputs muscle force location, direction and magnitude; joint contact location, direction and magnitude; and bite contact location, direction and magnitude for each biting simulation.

## 2.2. Finite-element analysis

The same CT dataset used to construct the MDA model was used to incorporate sutures into the skull. Sutures were integrated as a separate material by carefully tracing the gaps between the skull bone facets on the individual micro-CT slice images, so that all individual skull bones were completely isolated from one another (i.e. fully separated by the sutural soft tissue). This approach guaranteed that all sutures were represented in their entirety so that for loads to pass from one bone to another in the model it would have to pass through the sutural soft tissue material (three-dimensional model with sutures shown in figure 1).

The model was converted into a tetrahedral mesh consisting of 395 822 elements, constructed from solid (10 node) higher order elements. From these elements, 291 920 were assigned as bone and 103 902 were assigned as sutural soft tissue. Sensitivity studies (N. Curtis 2010, unpublished data) demonstrated that these were sufficient numbers of elements to accurately predict the strain through the model. Two set-ups were analysed: one representing fused sutures where the sutural soft tissue material was given the same material properties as bone (Young's modulus and Poisson's ratio of 17 and 0.3 GPa, respectively); and another representing patent sutures where the sutural soft tissue material was given a Young's modulus of 10 MPa and a Poisson's ratio of 0.3 MPa. All material properties were consistent with direct measurements and were within the ranges applied by other researchers [24,36–38,44,63–66].

A series of 15 FEAs was carried out on both the fused and patent suture models, with all muscle, joint and bite force locations, directions and magnitudes imported directly from the MDA simulations. Although theoretically all forces within the system should be in equilibrium, owing to the large number of individual forces, even small variations from the exact MDA locations of these applied forces would cause instability within the FEAs (i.e. there would be unconstrained full body motion of the model). Therefore, to ensure a stable FE solution, fixed constraints were included in the model. The locations of these constraints were taken at the joint and bite contacts as defined by the MDA (i.e. neck joint, jaw joints and bite point). One node at the neck location (occipital condyle) was constrained in the medial–lateral and anterior–posterior directions ($x$- and $z$-axes), one node at each jaw joint and bite point was constrained in the vertical direction ($y$-axis). These constraints were considered minimal, and restricted full body motion but not deformations of the skull. For example, the neck, bite and joint contact locations could all deform with respect to each other, and both jaw joint contact locations could deform relative to each other. After the FE solutions were complete, von Mises strains of all bone elements (291 920 elements) in the model were stored in element tables. A previous study carried out by Curtis et al. [36] showed von Mises strains to be a good indicator of bone performance. Investigating the strain in the sutural soft tissue material is beyond the scope of this study.

## 3. Results

### 3.1. Multibody dynamics analysis

The MDA simulations were similar to those carried out in a previous study, where more detailed results are presented [36]. From the MDA, muscle force locations, orientations and magnitudes; joint force locations, orientations and magnitudes; and bite force locations, orientations and magnitudes were predicted for 15 separate biting simulations (figure 2). Table 1 summarizes peak bite forces and joint forces predicted from the MDA. All predicted muscle, joint and bite forces were exported for use in the FEAs.

### 3.2. Finite-element analysis

Thirty separate FEAs were carried out on the same skull, 15 with sutures modelled as fused and 15 with sutures modelled as patent. In analyses where sutures were modelled as
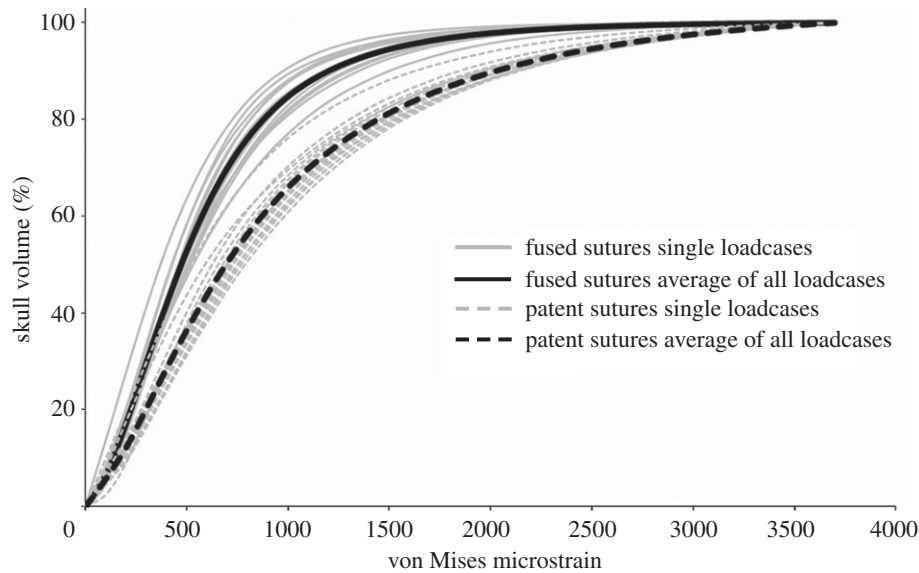
**Figure 3.** Cumulative strain plots showing the % volume of the skull (bone only not sutural soft tissue) at specific von Mises strain levels. Plots of all 15 individual loadcases along with the average of all loadcases are presented for both the fused and patent suture states.

**Table 1.** Bite forces and jaw joint forces predicted by the MDA. Total forces are shown for bilateral bites; therefore, the force on each side of the skull is approximately half that presented. Working refers to the force on the same side as the bite occurs, while balancing refers to the opposite side to which biting occurs. See figure 2 for explanation of bite locations.

| bite type | bite location | bite force (N) | working joint force (N) | balancing joint force (N) |
|---|---|---|---|---|
| bilateral | B1 | 121 | 540 | — |
| | B2 | 150 | 524 | — |
| | B3 | 165 | 510 | — |
| | B4 | 185 | 490 | — |
| | B5 | 214 | 462 | — |
| unilateral | U2 | 150 | 249 | 276 |
| | U3 | 166 | 232 | 276 |
| | U4 | 187 | 212 | 277 |
| | U5 | 216 | 183 | 278 |

fused, individual bites generated areas of both high and low strain throughout the skull, with higher strains concentrated around muscle attachments and bite points. In such cases, 53 per cent of the skull volume was at strain levels of less than 500 microstrain (figure 3). When sutures were modelled as patent, it was immediately obvious that strains in some of the low-level strain regions were elevated (figure 4), with only 37 per cent of the skull volume at strains of under 500 microstrain (figure 3). This was noted across all 15 separate bites, with overall mean element strain (i.e. the average strain value of each element) throughout the skull increasing from approximately 655 microstrain (fused sutures) to approximately 1226 microstrain (patent sutures). The percentage volume of bone within the skull at specific strain magnitudes was similar for all individual loading cases with each suture state (i.e. fused or patent), but the percentage of bone at lower strain levels was reduced considerably when sutures were patent (figure 3).

## 4. Discussion

The adult skull of the New Zealand reptile *Sphenodon* contains many patent sutures [3], making it an ideal subject for an investigation of the impact of these sutures on overall skull performance. We used a combination of MDA and FEA to load the skull and assess the impact of patent sutures on skull strains in *Sphenodon*. As with all computer modelling investigations, there are some approximations that could impact on the model performance. In our experience, their impact is probably small in relation to the effects we observe, but it is important to be explicit about potential modelling limitations. All sutures were carefully and accurately positioned throughout the skull, but to allow appropriate meshing within the FE model the sutures needed to be enlarged and simplified. The non-enlarged sutures were approximately 0.35 mm wide, whereas the enlarged suture width was approximately 0.5 mm, but this did vary slightly throughout the skull. Enlarging the sutures may have reduced the constraining properties of the sutures and their relative deformations may be greater than found in nature. Another approximation concerns the material properties of the bone and sutural soft tissue material. Both were represented as isotropic and homogeneous structures, which in reality is not the case. Although these approximations will have some effect on strains generated, they would not be expected to alter either the general strain patterns or the differences in magnitude between the fused and patent models. As such, the findings and conclusions of this investigation would not be affected.

Our findings falsify hypotheses 1 and 2 (outlined in §1) in that the presence of patent sutures clearly impacts on stress and strain distributions by raising strains in certain skull regions. Thus, our experiment indicates that patent sutures lead to a more consistent higher strain magnitude over the skull, substantially limiting low-strain regions when compared with a fused suture model. While increasing bone strains may seem counterproductive, it could be an important consequence of patent sutures. Bone strain is thought to be the stimulus for bone modelling/remodelling, and if strains are too low or too high, bone will be removed or deposited accordingly [67–71]. It is therefore important for bone strains
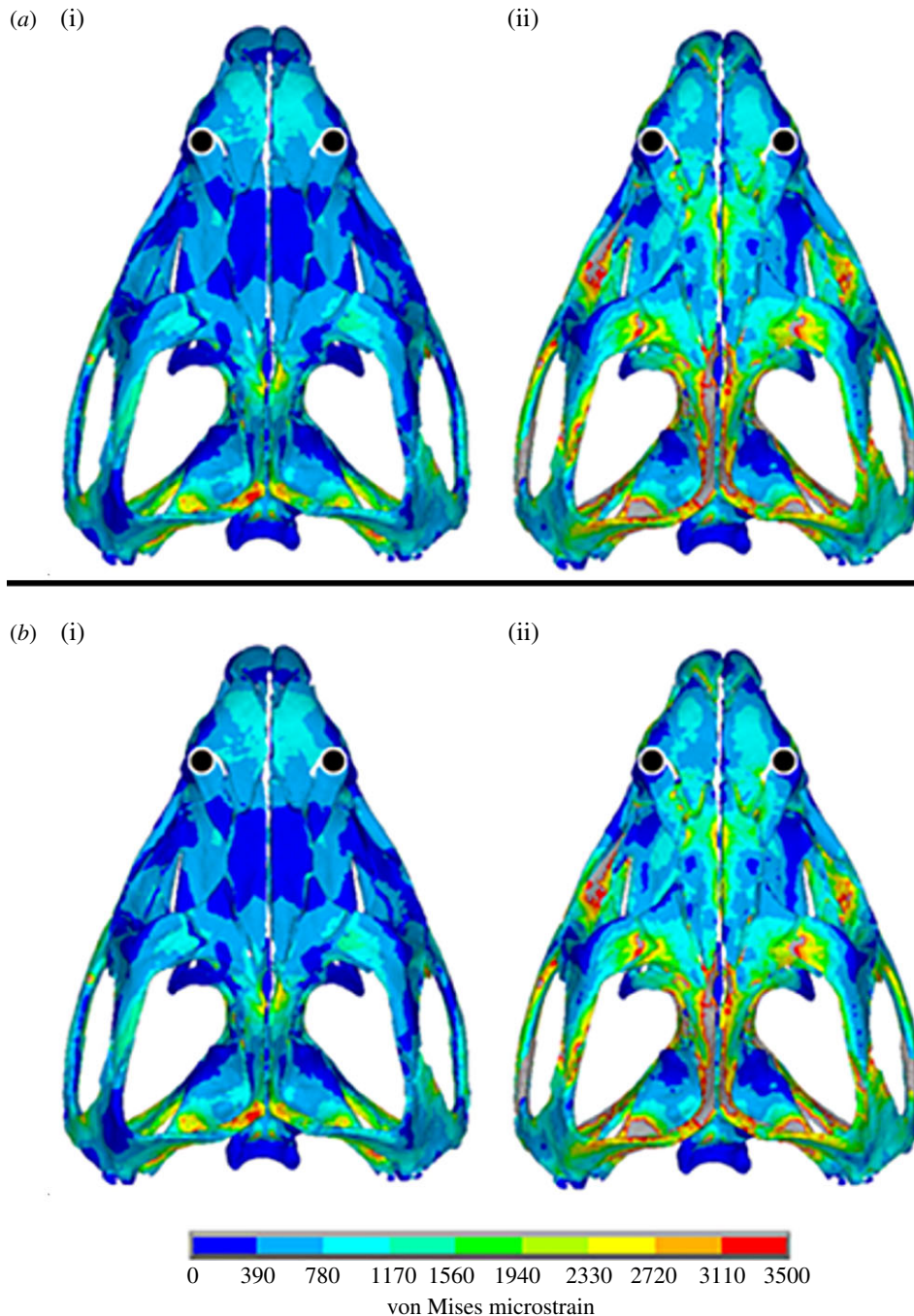
**Figure 4.** Sample von Mises strain distribution plots with (i) fused and (ii) patent suture states resulting from (*a*) an anterior bilateral bite and (*b*) a posterior unilateral bite. Black circle represents bite location. Suture material is not visible in these images.

to be within an *equilibrium window* of strain. When sutures were modelled as fused within our FE simulations large regions of the skull experienced very low-strain magnitudes during biting. Identifying exact bone remodelling strain magnitudes is problematic and thus we cannot say categorically that our predicted strains with patent sutures would reduce the incidence of bone resorption; however, we are confident that our predicted peak strains are consistent with those recorded *in vivo* and *in vitro*. Peak (principal) strain magnitudes of between 900 and 5200 microstrain have been reported in bone during forceful loading [72–75], including 2000–3000 microstrain in a pig skull [30,76]. We noted peak tensile and compressive strains of approximately 2000–3000 microstrain in our study (figure 5).

Consistent with hypothesis 3, introducing anatomically accurate patent sutures into our model raised the strains in the very low-strain regions of the skull, generating a more widely distributed, high level of strain (figure 4). Thus, patent sutures offer two potential benefits. The first is a reduction of gross strain gradients (i.e. large regions of the skull at low strains and other regions at high strains), which could indicate a reduction of bending or twisting in the skull. Bone is more likely to fail under tensile strains, and these occur most often when bone is under bending or torsion [77]. However, it should be noted that strain gradients could be related to deformation regimens other than bending or twisting. The second potential benefit is that during each individual bite, irrespective of location or type, the general distribution of strain is similar. This reduces the chance of an area of the skull being under loaded. In figure 4, localized red *hotspots* are evident on the patent suture model, which indicate areas of high strain. The majority of these *hotspots* appear at
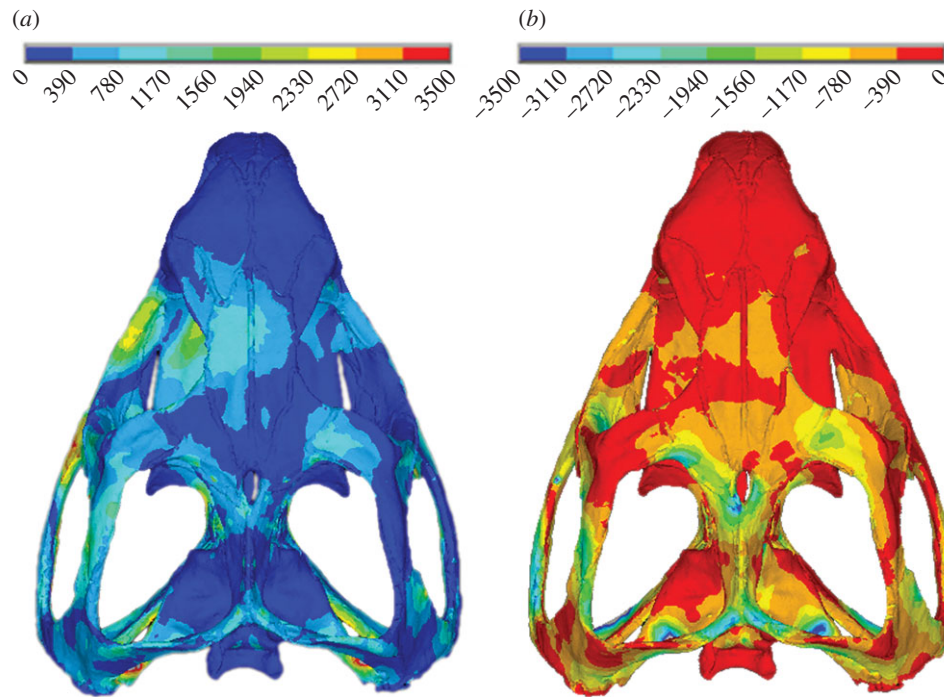
**Figure 5.** Example (*a*) first and (*b*) third principal strain plots for a single loadcase. Values in microstrain.

locations where the bone in the model is very thin adjacent to the sutures. These *hotspots* are likely to be a result of the modelling limitations discussed earlier, whereby some sutures were expanded slightly so that they could be modelled with a sufficient number of reasonably shaped elements.

During growth and development, bone adapts more readily than at any other time in the animal's life. Low strains at this stage could result in under-developed/under-ossified bony structures, and the careful modulation of skull strains ensures the careful modulation of skull growth. Generating higher levels of strain throughout the adult skull is also important, and may be why some sutures remain patent even when the skull has stopped growing. There are several reasons why an animal may not bite at all points along the jaw at equal frequency: animals often have preferential sides of the jaw on which they bite more frequently [78,79], and different foods may require differential use of the jaw for their capture and breakdown. Additionally, the generally high levels of strain throughout the skull could render it more resilient in the face of pathologies that affect biting; ensuring bone is not lost or weakened due to short-term functional impairment. We have shown in *Sphenodon* that without patent sutures in the cranium the skull bones would only experience low-level strains, which could reduce their resistance to fracture.

These findings agree with previous studies on reptiles that suggest patent sutures modify strains substantially throughout the skull during biting [24]. However, the results are at variance with experimental and modelling studies on mammals that suggest some regions of the mammalian skull experience only very low strains during mastication [31,80]. Similarly, computer models of mammal skulls with some patent sutures do not differ significantly from skulls with no (or completely fused) sutures [52]. However, further discussion must await the analysis of a comparable mammalian skull with a full complement of patent sutures.

We hypothesize that most of the bone in the space-frame-type structure of the *Sphenodon* cranium is loaded principally through feeding activities and neck musculature, where the forces are intermittent but relatively high. Although equivalent biting and neck loads will also be experienced by a large part of the stiffened-shell-type cranium of mammals, other areas may experience lower magnitude but higher frequency loads. It may be these high-frequency–low-magnitude loads that help maintain bone in the low-strain areas in mammal skulls [71].

In conclusion, the results of this analysis reveal for the first time that patent sutures help reduce the number of areas of low-level strain throughout the reptile skull, leading to a more predictable and widely distributed high level of strain during every bite. This has important implications with respect to bone growth and remodelling in both juvenile and adult skulls, ensuring that bone grows (and is maintained) normally and optimally.

# References

1. Herring SW. 1972 Sutures: a tool in functional cranial analysis. *Acta Anat.* (*Basel*) **83**, 222–247. (doi:10.1159/000143860)

2. Herring SW. 2008 Mechanical influences on suture development and patency. *Front. Oral Biol.* **12**, 41–56. (doi:10.1159/000115031)

3. Jones MEH, Curtis N, Fagan MJ, O'Higgins P, Evans SE. 2011 Hard tissue anatomy of the cranial joints in *Sphenodon* (Rhynchocephalia): sutures, kinesis,

and skull mechanics. *Palaeontol. Electron.* 14.2.17A. (doi:10.1017/CBO9780511793752)

4. Koskinen L, Isotupa K, Kosko K. 1975 A note on craniofacial suture growth. *Am. J. Phys. Anthropol.* **45**, 511–516. (doi:10.1002/ajpa.1330450312)

5. Pritchard JJ, Scott JH, Girgis FG. 1956 The structure and development of cranial and facial sutures. *J. Anat.* **90**, 73–86.

6. Sun Z, Lee E, Herring SW. 2004 Cranial sutures and bones: growth and fusion in relation to masticatory strain. *Anat. Rec.* **276A**, 150–161. (doi:10.1002/ar.a.20002)

7. Mao JJ. 2002 Mechanobiology of craniofacial sutures. *J. Dent. Res.* **81**, 810–816. (doi:10.1177/154405910208101203)

8. Jaslow CR. 1990 Mechanical properties of cranial sutures. *J. Biomech.* **23**, 313–321. (doi:10.1016/0021-9290(90)90059-C)

9. Cohen MM. 2000 Sutural biology, ch. 2. In *Craniosynostosis* (eds MM Cohen, RE Mclean), pp. 11–23. Oxford, UK: University Press.

10. Opperman LA. 2000 Cranial sutures as intramembranous bone growth sites. *Dev. Dyn.* **219**, 472–485. (doi:10.1002/1097-0177(2000)9999:9999<::AID-DVDY1073>3.0.CO;2-F)

11. Oudhof HAJ. 1982 Sutural growth. *Acta Anat. (Basel)* **112**, 58–68. (doi:10.1159/000145497)

12. Persson M. 1995 The role of sutures in normal and abnormal craniofacial growth. *Acta Odontol. Scand.* **53**, 152–161. (doi:10.3109/00016359509005965)

13. Adamo MA, Pollack IF. 2009 Current management of craniosynostosis. *Neurosurg. Q.* **19**, 82–87. (doi:10.1097/WNQ.0b013e3181a32e1e)

14. Brunner S, Bryden MM, Shaughnessy PD. 2004 Cranial ontogeny of otariid seals. *Syst. Biodivers.* **2**, 83–110. (doi:10.1017/S1477200004001367)

15. Cohen MMJ, Kreiborg S. 1998 Suture formation, premature sutural fusion, and suture default zones in Apert syndrome. *Am. J. Med. Genet.* **62**, 339–344. (doi:10.1002/(SICI)1096-8628(19960424)62:4<339::AID-AJMG3>3.0.CO;2-M)

16. David L, Glazier S, Pyle J, Thompson J. 2009 Classification system for sagittal craniosynostosis. *J. Craniofac. Surg.* **20**, 279–282. (doi:10.1097/SCS.0b013e3181945ab0)

17. Morriss-Kay GM, Wilkie AOM. 2005 Growth of the normal skull vault and its alteration in craniosynostosis: insights from human genetics and experimental studies. *J. Anat.* **207**, 637–653. (doi:10.1111/j.1469-7580.2005.00475.x)

18. Wang Q, Strait DS, Dechow PC. 2006 Fusion patterns of craniofacial sutures in rhesus monkey skulls of known age and sex from Cayo Santiago. *Am. J. Phys. Anthropol.* **131**, 469–485. (doi:10.1002/ajpa.20481)

19. Moss ML. 1961 Extrinsic determination of sutural area morphology in the rat calvaria. *Acta Anat. (Basel)* **44**, 263–272. (doi:10.1159/000141726)

20. Gussekloo SWS, Vosselman MG, Bout RG. 2001 Three-dimensional kinematics of skeletal elements in avian prokinetic and rhynchokinetic skulls

determined by Roentgen stereophotogrammetry. *J. Exp. Biol.* **204**, 1735–1744.

21. Iordansky NN. 1990 Evolution of cranial kinesis in lower tetrapods. *Neth. J. Zool.* **40**, 32–54. (doi:10.1163/156854289X00174)

22. Buckland-Wright JC. 1972 The shock absorbing effect of cranial sutures in certain mammals. *J. Dent. Res.* **51**, 1241.

23. Rafferty KL, Herring SW, Marshall CD. 2003 Biomechanics of the rostrum and the facial sutures. *J. Morphol.* **257**, 33–44. (doi:10.1002/jmor.10104)

24. Moazen M, Curtis N, O'Higgins P, Jones MEH, Evans SE, Fagan MJ. 2009 Assessment of the role of sutures in a lizard skull: a computer modeling study. *Proc. R. Soc. B* **276**, 39–46. (doi:10.1098/rspb.2008.0863)

25. Rayfield EJ. 2004 Cranial mechanics and feeding in *Tyrannosaurus rex*. *Proc. R. Soc. Lond. B* **271**, 1451–1459. (doi:10.1098/rspb.2004.2755)

26. Rayfield EJ. 2005 Aspects of comparative cranial mechanics in the theropod dinosaurs *Coelophysis*, *Allosaurus* and *Tyrannosaurus*. *Zool. J. Linn. Soc.* **144**, 309–316. (doi:10.1111/j.1096-3642.2005.00176.x)

27. Reed AD, Porro LB, Iriarte-Diaz J, Lemberg JB, Holliday CM, Anapol F, Ross CF. 2011 The impact of bone and suture material properties on mandibular function in *Alligator mississippiensis*: testing theoretical phenotypes with finite element analysis. *J. Anat.* **218**, 59–74. (doi:10.1111/j.1469-7580.2010.01319.x)

28. Moss ML, Salentijn L. 1969 The capsular matrix. *Am. J. Orthod. Dentofacial Orthop.* **56**, 474–490.

29. Behrents RG, Carlson DS, Abdelnour T. 1978 *In vivo* analysis of bone strain about the sagittal suture in *Macaca mulatta* during masticatory movements. *J. Dent. Res.* **57**, 904–908. (doi:10.1177/00220345780570091401)

30. Herring SW, Mucci RJ. 1991 *In vivo* strain in cranial sutures: the zygomatic arch. *J. Morphol.* **207**, 225–239. (doi:10.1002/jmor.1052070302)

31. Hylander WL, Johnson KR. 1997 *In vivo* strain patterns in the zygomatic arch of macaques and the significance of these patterns for functional interpretations of craniofacial form. *Am. J. Phys. Anthropol.* **102**, 203–232. (doi:10.1002/(SICI)1096-8644(199702)102:2<203::AID-AJPA5>3.0.CO;2-Z)

32. Popowics TE, Herring SW. 2007 Load transmission in the nasofrontal suture of the pig, *Sus scrofa*. *J. Biomech.* **40**, 837–844. (doi:10.1016/j.jbiomech.2006.03.011)

33. Ravosa MJ, Noble VE, Hylander WL, Johnson KR, Kowalski EM. 2000 Masticatory stress, orbital orientation and the evolution of the primate postorbital bar. *J. Hum. Evol.* **38**, 667–693. (doi:10.1006/jhev.1999.0380)

34. Ross CF, Berthaume MA, Dechow PC, Iriarte-Diaz J, Porro LB, Richmond BG, Spencer MA, Strait DS. 2011 *In vivo* bone strain and finite-element modeling of the craniofacial haft in catarrhine primates. *J. Anat.* **218**, 112–141. (doi:10.1111/j.1469-7580.2010.01322.x)

35. Wang Q, Dechow PC, Wright BW, Ross CF, Strait DS, Richmond BG, Spencer MA, Byron CD. 2008 Surface strain on bone and sutures in a monkey facial skeleton: an *in vitro* method and its relevance to finite element analysis. In *Primate craniofacial function and biology* (eds CJ Vinyard, MJ Ravosa, CE Wall), pp. 149–172. New York, NY: Springer.

36. Curtis N, Jones MEH, Shi J, O'Higgins P, Evans SE, Fagan MJ. 2011 Functional relationship between skull form and feeding mechanics in *Sphenodon*, and implications for diapsid skull development. *PLoS ONE* **6**, e29804. (doi:10.1371/journal.pone.0029804)

37. Curtis N, Kupczik K, O'Higgins P, Moazen M, Fagan MJ. 2008 Predicting skull loading: applying multibody dynamics analysis to a macaque skull. *Anat. Rec.* **291**, 491–501. (doi:10.1002/ar.20689)

38. Curtis N, Witzel U, Fitton L, O'Higgins P, Fagan MJ. 2011 The mechanical significance of the temporal fasciae in *Macaca fascicularis*: an investigation using finite element analysis. *Anat. Rec.* **294**, 1178–1190. (doi:10.1002/ar.21415)

39. Dumont ER, Davis JL, Grosse IR, Burrows AM. 2011 Finite element analysis of performance in the skulls of marmosets and tamarins. *J. Anat.* **218**, 151–162. (doi:10.1111/j.1469-7580.2010.01247.x)

40. McHenry CR, Wroe S, Clausen PD, Moreno K, Cunningham E. 2007 Supermodeled sabercat, predatory behavior in *Smilodon fatalis* revealed by high-resolution 3D computer simulation. *Proc. Natl Acad. Sci. USA* **104**, 16 010–16 015. (doi:10.1073/pnas.0706086104)

41. Moazen M, Curtis N, O'Higgins P, Evans SE, Fagan MJ. 2009 Biomechanical assessment of evolutionary changes in the lepidosaurian skull. *Proc. Natl Acad. Sci. USA* **106**, 8273–8277. (doi:10.1073/pnas.0813156106)

42. Moreno K, Wroe S, Clausen PD, McHenry CR, D'Amore DC, Rayfield EJ, Cunningham E. 2008 Cranial performance in the Komodo dragon (*Varanus komodoensis*) as revealed by high-resolution 3-D finite element analysis. *J. Anat.* **212**, 736–746. (doi:10.1111/j.1469-7580.2008.00899.x)

43. Preuschoft H, Witzel U. 2004 A biomechanical approach to craniofacial shape in primates, using FESA. *Ann. Anat.* **186**, 397–404. (doi:10.1016/S0940-9602(04)80071-2)

44. Witzel U, Preuschoft H. 2005 Finite-element model construction for the virtual synthesis of the skulls in vertebrates: case study of *Diplodocus*. *Anat. Rec.* **283**, 391–401. (doi:10.1002/ar.a.20174)

45. Farke AA. 2008 Frontal sinuses and head-butting in goats: a finite element analysis. *J. Exp. Biol.* **211**, 3085–3094. (doi:10.1242/jeb.019042)

46. Bright JA, Gröning F. 2011 Strain accommodation in the zygomatic arch of the pig: a validation study using digital speckle pattern interferometry and finite element analysis. *J. Morphol.* **272**, 1388–1398. (doi:10.1002/jmor.10991)

47. Bright JA. 2012 The importance of craniofacial sutures in biomechanical finite element models of the domestic pig. *PLoS ONE* **7**, e31769. (doi:10.1371/journal.pone.0031769)

48. Jasinoski SC, Rayfield EJ, Chinsamy A. 2010 Functional implications of dicynodont cranial suture morphology. *J. Morphol.* **271**, 705–728.

49. Jasinoski SC, Reddy BD, Louw KK, Chinsamy A. 2010 Mechanics of cranial sutures using the finite element method. *J. Biomech.* **43**, 3104–3111. (doi:10.1016/j.jbiomech.2010.08.007)

50. Wang Q, Wood S, Grosse I, Ross C, Zapata U, Byron C, Wright B, Strait D. 2012 The role of the sutures in biomechanical dynamic simulation of a macaque cranial finite element model: implications for the evolution of craniofacial form. *Anat. Rec.* **295**, 278–288. (doi:10.1002/ar.21532)

51. Moazen M, Costantini D, Bruner E. 2013 A sensitivity analysis to the role of the fronto-parietal suture in *Lacerta bilineata*: a preliminary finite element study. *Anat. Rec.* **296**, 198–209.

52. Wang Q, Smith AL, Strait DS, Wright BW, Richmond BG, Grosse IR, Byron CD, Zapata U. 2010 The global impact of sutures assessed in a finite element model of a macaque cranium. *Anat. Rec.* **293**, 1477–1491. (doi:10.1002/ar.21203)

53. Metzger KA, Daniel WJT, Ross CF. 2005 Comparison of beam theory and finite-element analysis with *in vivo* bone strain data from the alligator cranium. *Anat. Rec.* **283**, 331–348. (doi:10.1002/ar.a.20167)

54. Ross CF, Metzger KA. 2004 Bone strain gradients and optimization in vertebrate skulls. *Ann. Anat.* **186**, 387–396. (doi:10.1016/S0940-9602(04)80070-0)

55. Herring SW, Teng S. 2000 Strain in the braincase and its sutures during function. *Am. J. Phys. Anthropol.* **112**, 575–593. (doi:10.1002/1096-8644(200008)112:4<575::AID-AJPA10>3.0.CO;2-0)

56. Thomason JJ, Grovum LE, Deswysen AG, Bignell WW. 2001 *In vivo* surface strain and sterology of the frontal and maxillary bones of sheep: implications for the structural design of the mammalian skull. *Anat. Rec.* **264**, 325–338. (doi:10.1002/ar.10025)

57. Curtis N, Jones MEH, Evans SE, O'Higgins P, Fagan MJ. 2009 Visualising muscle anatomy using three-dimensional computer models: an example using the head and neck muscles of *Sphenodon*. *Palaeontol. Electron.* **12**, article no. 12.3.7T. See http://palaeo-electronica.org/2009_3/194/index.html.

58. Curtis N, Jones MEH, Evans SE, Shi J, O'Higgins P, Fagan MJ. 2010 Predicting muscle activation patterns from motion and anatomy: modelling the skull of *Sphenodon* (Diapsida: Rhynchocephalia).

*J. R. Soc. Interface* **7**, 153–160. (doi:10.1098/rsif.2009.0139)

59. Curtis N, Jones MEH, Lappin AK, O'Higgins P, Evans SE, Fagan MJ. 2010 Comparison between *in vivo* and theoretical bite performance: using multi-body modelling to predict muscle and bite forces in a reptile skull. *J. Biomech.* **43**, 2804–2809. (doi:10.1016/j.jbiomech.2010.05.037)

60. Jones MEH, Curtis N, O'Higgins P, Fagan MJ, Evans SE. 2009 The head and neck muscles associated with feeding in *Sphenodon* (Reptilia: Lepidosauria: Rhynchocephalia). *Palaeontol. Electron.* **12**, article no. 12.2.7A. See http://palaeo-electronica.org/2009_2/179/index.html.

61. Jones MEH, O'Higgins P, Fagan M, Evans SE, Curtis N. 2012 Shearing mechanics and the influence of a flexible symphysis during oral food processing in *Sphenodon* (Lepidosauria: Rhynchocephalia). *Anat. Rec.* **295**, 1075–1091. (doi:10.1002/ar.22487)

62. Curtis N, Jones MEH, Evans SE, O'Higgins P, Fagan MJ. 2010 Feedback control from the jaw joints during biting: an investigation of the reptile *Sphenodon* using multibody modelling. *J. Biomech.* **43**, 3132–3137. (doi:10.1016/j.jbiomech.2010.08.001)

63. Strait DS, Wang Q, Dechow PC, Ross CF, Richmond BG, Spencer MA, Patel BA. 2005 Modeling elastic properties in finite element analysis: how much precision is needed to produce an accurate model? *Anat. Rec.* **283**, 275–287. (doi:10.1002/ar.a.20172)

64. Kupczik K, Dobson CA, Fagan MJ, Crompton RH, Oxnard CE, O'Higgins P. 2007 Assessing mechanical function of the zygomatic region in macaques: validation and sensitivity testing of finite element models. *J. Anat.* **210**, 41–53. (doi:10.1111/j.1469-7580.2006.00662.x)

65. Dumont ER, Grosse IR, Slater GJ. 2009 Requirements for comparing the performance of finite element models of biological structures. *J. Theor. Biol.* **256**, 96–103. (doi:10.1016/j.jtbi.2008.08.017)

66. Wang Q, Wright BW, Smith A, Chalk J, Byron CD. 2010 Mechanical impact of incisor loading on the primate midfacial skeleton and its relevance to human evolution. *Anat. Rec.* **293**, 607–617. (doi:10.1002/ar.21123)

67. Carter DR. 1984 Mechanical loading histories and cortical bone remodeling. *Calcif. Tissue Int.* **39**, 19–24. (doi:10.1007/BF02406129)

68. Frost HM. 1987 Bone 'mass' and the 'mechanostat': a proposal. *Anat. Rec.* **219**, 1–9. (doi:10.1002/ar.1092190104)

69. Lanyon LE. 1982 Mechanical function and bone remodeling. In *Bone in clinical orthopaedics* (ed G. Sumner-Smith). Philadelphia, PA: Saunders.

70. Lanyon LE, Skerry T. 2001 Postmenopausal osteoporosis as a failure of bone's adaptation to functional loading: a hypothesis. *J. Bone Miner. Res.* **16**, 1937–1947. (doi:10.1359/jbmr.2001.16.11.1937)

71. Turner CH. 1998 Three rules for bone adaptation to mechanical stimuli. *Bone* **23**, 399–407. (doi:10.1016/S8756-3282(98)00118-5)

72. Biewener AA, Thomason JJ, Lanyon LE. 1983 Mechanics of locomotion and jumping in the forelimb of the horse (*Equus*): *in vivo* stress developed in the radius and metacarpus. *J. Zool. Lond.* **201**, 67–82. (doi:10.1111/j.1469-7998.1983.tb04261.x)

73. Nunemaker DM, Butterweck DM, Provost MT. 1990 Fatigue fractures in thoroughbred racehorses: relationships with age, peak bone strain and training. *J. Orthop. Res.* **8**, 604–611. (doi:10.1002/jor.1100080417)

74. O'Connor JA, Lanyon LE, MacFie H. 1982 The influence of strain rate on adaptive remodelling. *J. Biomech.* **15**, 767–781. (doi:10.1016/0021-9290(82)90092-6)

75. Rubin CT, Lanyon LE. 1984 Regulation of bone formation by applied dynamic loads. *J. Bone Joint Surg.* **66-A**, 397–402.

76. Herring SW, Pedersen SC, Huang X. 2005 Ontogeny of bone strain: the zygomatic arch in pigs. *J. Exp. Biol.* **208**, 4509–4521. (doi:10.1242/jeb.01923)

77. Currey JD. 2002 *Bones: structure and mechanics*. Princeton, NJ: Princeton University Press.

78. Diernberger S, Bernhardt O, Schwahn C, Kordass B. 2008 Self-reported chewing side preference and its associations with occlusal, temporomandibular and prosthodontic factors: results from the population-based Study of Health in Pomerania (SHIP-0). *J. Oral Rehabil.* **35**, 613–620. (doi:10.1111/j.1365-2842.2007.01790.x)

79. Martinez-Gomis J, Lujan-Climent M, Palau S, Bizar J, Salsench J, Peraire M. 2009 Relationship between chewing side preference and handedness and lateral asymmetry of peripheral factors. *Arch. Oral Biol.* **54**, 101–107. (doi:10.1016/j.archoralbio.2008.09.006)

80. Ross CF. 2001 *In vivo* function of the craniofacial haft: the interorbital 'pillar'. *Am. J. Phys. Anthropol.* **116**, 108–139. (doi:10.1002/ajpa.1106)

# Correction

# Cranial sutures work collectively to distribute strain throughout the reptile skull

Neil Curtis, M. E. H. Jones, S. E. Evans, P. O'Higgins and M. J. Fagan

Figure 4 was presented incorrectly, with (*a*) and (*b*) displaying the same bite position. The corrected figure below shows different bite positions for (*a*) and (*b*) as was initially intended.
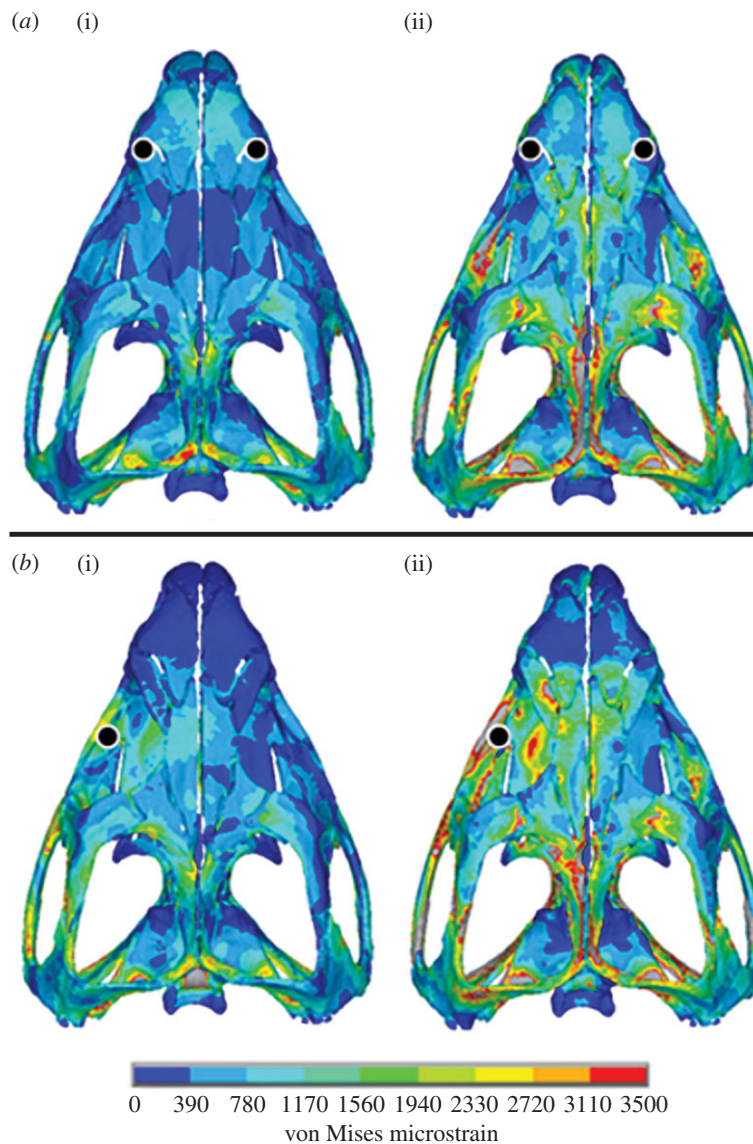


**Figure 4.** Sample von Mises strain distribution plots with (i) fused and (ii) patent suture states resulting from (*a*) an anterior bilateral bite and (*b*) a posterior unilateral bite. Black circle represents bite location. Suture material is not visible in these images.